

HELIUM INDUCED DEGRADATION IN THE WELDABILITY OF AN AUSTENITIC STAINLESS STEEL*

H. T. Lin¹, S. H. Goods², M. L. Grossbeck³, and B. A. Chin¹

1. Auburn University. 2. Sandia National Laboratories, Livermore, 3. Oak Ridge National Laboratory

ABSTRACT: Autogenous gas tungsten arc welding was performed on He-doped type 316 stainless steel. Helium was uniformly implanted in the material using the "tritium trick" to levels of 27 and 105 appm. Severe intergranular cracking occurred in both fusion and heat-affected zones. Microstructural observations of the fusion zone indicated that the pore size, degree of porosity, and tendency to form cracks increased with increasing helium concentration. Scanning electron microscopy showed that cracking in He-doped materials was due to the precipitation of helium bubbles on grain boundaries and dendrite interfaces. Results of the present study demonstrate that the use of conventional welding techniques to repair materials degraded by exposure to radiation may be difficult if the irradiation results in the generation of even rather small amounts of helium.

KEY WORDS: Tritium Trick, He-Doped Materials, Gas Tungsten Arc Welding, Heat-Affected Zone Cracking, Intergranular Fracture.

*Research Sponsored by the Office of Fusion Energy, U. S. Department of Energy under contract DE-AC05-84OR21400 with the Martin Marietta Energy Systems, Inc., and Sandia National Laboratories, Livermore under contract DE-AC04-76DP00789

The submitted manuscript has been authored by a contractor of the U.S. Government under contract No. DE-AC05-84OR21400. Accordingly, the U.S. Government retains a nonexclusive, royalty-free license to publish or reproduce the published form of this contribution, or allow others to do so, for U.S. Government purposes.

MASTER

DISCLAIMER

This report was prepared as an account of work sponsored by an agency of the United States Government. Neither the United States Government nor any agency thereof, nor any of their employees, makes any warranty, express or implied, or assumes any legal liability or responsibility for the accuracy, completeness, or usefulness of any information, apparatus, product, or process disclosed, or represents that its use would not infringe privately owned rights. Reference herein to any specific commercial product, process, or service by trade name, trademark, manufacturer, or otherwise does not necessarily constitute or imply its endorsement, recommendation, or favoring by the United States Government or any agency thereof. The views and opinions of authors expressed herein do not necessarily state or reflect those of the United States Government or any agency thereof.

INTRODUCTION

The exposure of metallic materials, such as structural components of the first wall and blanket of fusion reactors, to high-energy (14 Mev) neutron irradiation will induce changes in both the material composition as well as its microstructure. Along with these changes may come a corresponding deterioration in corrosion resistance and mechanical properties. It is not unreasonable, therefore, to expect that the repair and replacement of degraded reactor components will be necessary. Such repairs may require the joining of irradiated materials through the use of conventional welding techniques.

One of the most important considerations in determining the post-irradiation weldability of a material is the fact that the exposure of a material to neutron irradiation will result in the production of entrapped helium. This helium is generated as the result of (n,α) reactions with the alloy constituents [1,2]. The very low solubility of helium in metals [3,4] results in its tendency to precipitate out as bubbles. Preferred nucleation sites for the helium bubbles are inhomogeneities such as precipitate interfaces, dislocations, and most importantly, grain boundaries. At elevated temperatures, these bubbles will grow rapidly under the influence of either internal or external (creep) stresses, weakening the grain boundaries. As these bubbles coalesce along the boundaries, intergranular fracture occurs. Since welding processes produce internal stresses (and elevated temperatures), the entrapped helium may severely affect the weldability and post-weld properties of the irradiated

material. Furthermore, welding produces severe gradients in both stress and temperature which may enhance the growth rate of helium bubbles further degrading the material properties [5].

In fact, attempts to repair stress corrosion cracks in an irradiated reactor tank containing several appm (atomic parts per million) helium by Gas Tungsten Arc (GTA) welding have proven to be difficult [6]. Recent examination of these welds has revealed the existence of grain boundary cracking in the heat-affected zone (HAZ) of the welds [7]. Because of the obviously hostile environment, detailed analysis of these welding induced defects has proven to be extremely difficult. Developing a quantitative understanding of the relationship between helium and weld cracking is virtually impossible due to difficulty in performing in-situ welding and subsequent analysis. The radiological hazards associated with the handling of these materials limits the scope of such studies and insures that they will be extremely costly.

The present study was carried out to provide a quantitative background for understanding the effects of helium on the subsequent weldability of materials. To avoid hot cell investigations which are both lengthy and expensive, welding performed on He-doped material was chosen to simulate the principal effects which occur during the joining of irradiated material. Helium was implanted into the test material via the "tritium trick". Type 316 stainless steel was chosen for the study because of the extensive data base, for both unirradiated and irradiated materials, detailing its microstructure and

properties.

EXPERIMENTAL PROCEDURE

The material studied in this program was Type 316 stainless steel (reference heat 8092297) of the U. S. Fast Breeder Reactor Program [8]. The chemical composition is listed in Table 1. The initial cold rolled 1.52 mm plate stock was annealed at 1050°C for one hour in inert gas. It was then cold-rolled to 0.76 mm followed by a final anneal at 1050°C which resulted in a fully recrystallized microstructure with a grain size of 70 μm . To produce the desired concentrations of helium in a relatively short period and minimize radioactive hazards after implantation, the "tritium trick" technique [9] was employed wherein helium is generated within a metal through the radioactive decay of tritium (tritium undergoes the decay reaction ${}^3\text{H} \rightarrow \beta^- + {}^3\text{He}$, and has a 12.3 yr half-life). In order to dope the low helium content specimens, the stainless steel sheet stock was exposed to tritium gas at a pressure of 38 MPa for 30 days at 300°C. Since the diffusivity of tritium in stainless steel is rapid at 300°C [10], this charging period ensured that a uniform concentration of tritium (and therefore a uniform distribution of helium) was established through the thickness of the starting material. At the end of this period, the exposed material was removed from the high pressure charging vessel and outgassed at 400°C at 10^{-3} Pa in order to stop further generation of helium and to remove residual tritium. In order to achieve the higher helium content, the same procedure was followed except that a tritium charging

pressure of 125 MPa was used. The concentrations of helium were then measured quantitatively using a vacuum fusion mass spectrographic technique [11] and were found to be 27 and 105 appm respectively.

Autogenous bead-on-plate welds were made using gas tungsten arc welding. Figure 1 shows the welding station that was located in a high velocity airhood with an air flow rate of 1.5 m/s. The semiautomatic motion of the welding torch was driven and controlled by a Unislide 8201M stepping motor controller. Welding was performed at 10 VDC, 24 A at a travel speed of 3.6 mm/sec under a protective argon atmosphere. Full penetration welds were produced in the 0.76 mm thick plate. The plates were laterally constrained during welding.

Metallographic sections transverse to the welding direction were prepared in order to study the weld microstructure. The specimen cross-sections were electrolytically etched in a solution of 40% HNO₃ and 60% H₂O.

To study mechanical properties of the welds, tensile tests were performed on an Instron mechanical testing machine at an initial strain rate of $5 \times 10^{-4} \text{ sec}^{-1}$. Tests were conducted at temperatures between 25 and 700°C in a vacuum of $4 \times 10^{-5} \text{ Pa}$. Fractographic analysis of fractured tensile specimens and weld cracks was conducted using a JEOL JSM-35CF scanning electron microscope.

RESULTS

Weld Response

Figures 2 and 3 show the morphological features of the as-welded materials with helium levels of 27 and 105 appm respectively. In the low helium content material, continuous through-thickness cracking in the HAZ was observed in 75% of the welded plates (6 out of 8). In the remaining plates, the cracking was discontinuous. Typically, this cracking occurred in the HAZ immediately adjacent to the fusion zone and was intergranular in nature (Figure 2b). In the higher helium content material, all of the welded plates (9 out of 9) showed HAZ cracking; in addition, more than half of the welded plates (6 out of 9) exhibited evidence of centerline cracking in the fusion zone as well. As in the previous instance, the HAZ cracking was fully intergranular in nature (Figure 3b) and occurred very near to the weld interface. Since no external loads were applied, in all cases, the cracking resulted from shrinkage stresses as the laterally constrained plates cooled after welding.

Features of weld crack surfaces in the HAZ and fusion zone were studied in detail using scanning electron microscopy. Figures 2 and 3 show these typical surface features. As stated above, the weld cracking was entirely intergranular in nature, and at higher magnification the grain boundary facets were observed to be decorated with a uniform distribution of dimples (Figures 2c and 3c). The average dimple size was approximately 1 μm and was the same for both the high and low helium content specimens. However, the dimple morphology (symmetry and spacing) observed on grain facets varied with the orientation of the grain boundaries with respect to thermal stresses in the HAZ. The

dimples on the exposed facets exhibited symmetrical features which indicated that they were formed from cavities that grew under the action of stresses normal to the boundary. Incipient cracking, arising from coalescence of cavities, was also observed along the grain boundary intersections (Figures 2c and 3c). The shear ligaments separating the dimples have been rounded by surface diffusion, indicating that the cracking occurred at high temperatures. Examination of the fusion zone centerline cracking indicated that the brittle failure proceeded along an interdendritic path during material resolidification (Figure 3d). Isolated spherical pores resulting from the precipitation of the entrapped helium were also observed on the interdendritic fracture surface.

Figure 4 shows the optical metallography of the welds from a section taken transverse to the welding direction for the 27 and 105 appm helium materials. A small amount of ferrite precipitation was observed near the fusion boundary. Generally, the microstructure of the fusion zone was primary austenite with visible spherical pores decorating the solidification dendrite boundaries. It is clear by comparing Figure 4b and c that the degree and size of the porosity was greater in the material containing 105 appm helium than in the lower helium concentration plates. The size of visible pores ranged from 0.5 to 70 μm . The larger pores were preferentially located in the fusion zone close to fusion boundary. The tendency to form bigger bubbles adjacent to the weld interface suggests that convective flow patterns in the weld pool act to sweep the helium toward that region, and the

stagnant flow in the weld interface enhances bubble coalescence.

The degree to which the pores decorated the dendritic interfaces is more clearly shown in Figure 5 where once again it is seen that the size and extent of porosity increased with increasing helium content. As no such porosity occurred in helium free stainless steel welded under identical conditions, it is reasonable to conclude that the spherical pores observed in the fusion zone are helium bubbles.

As shown in Figure 4, the metallographic analysis revealed that the intergranular cracking occurred in the HAZ close to the weld interface. Within this narrow zone, secondary cracking away from the main fracture was observed along with porosity on the grain boundaries. Fracture appeared therefore to occur due to the growth and coalescence of helium bubbles along grain boundaries. This is obviously the region of solid material which experiences the combination of the highest temperatures and the highest shrinkage stresses required to induce the cracking phenomenon.

Mechanical Properties

Results of tensile tests on welded control and He-doped specimens as a function of test temperature are shown in Figures 6 through 8. For comparison purposes, tensile results of unwelded control (parent metal) and He-doped specimens are also shown. Tensile specimens of welded materials were prepared using a punch and die in an orientation transverse to the welding direction. The portion in the center of the gage section

contained both fusion and HAZ zones in approximately 50 % of the gage length (12.7 mm).

The tensile results indicated that yield strength decreased linearly with increasing temperature for all cases (Figure 6). The He-doped materials have the same yield strength as the undoped materials indicating no strengthening effect was incurred by the presence of helium. There was a significant increase in the yield strength of the welded materials relative to unwelded parent specimens.

In all cases, the ultimate tensile strength (UTS) decreased with increasing test temperatures (Figure 7). For unwelded materials, the results reveal that the UTS was insensitive to the presence of helium at these concentrations. The strength of the welded control (no helium) was the same as that of the unwelded control at room temperature. However, it was somewhat less at the elevated test temperatures. The UTS of the He-bearing specimens subsequent to welding was severely degraded relative to welded control, unwelded control and unwelded He-doped materials. In fact, the UTS of the welded He-doped specimens was virtually identical to their yield strengths (Table II), indicating that the specimens failed immediately upon yielding.

Prior to welding, the He-doped specimens had the same ductility as the unwelded control specimens up to 600°C (Figure 8). At 700°C the total elongation of unwelded, He-doped specimens decreased with increasing helium content but never fell below 10%. The ductility of all welded specimens was found to be lower than that of unwelded specimens. This is due to the fact

that the deformation and fracture is restricted to the fusion zone. The welded, He-doped specimens showed the lowest ductilities, generally less than 2% and as low as 0.2%. All welded, He-doped specimens failed at the fusion boundary. A typical fracture surface of a welded specimen containing 27 appm He tested at room temperature is shown in Figure 9. The fracture surface was nearly 100 percent intergranular, and at high magnification the grain boundary facets exhibited a dimple structure that was quite similar to the weld crack surface in the HAZ. The main difference was that the dimple shear walls were much more sharply defined as the result of room temperature fracture.

DISCUSSION

Weld Response, HAZ

The scanning electron micrographs of the welded material revealed that the brittle intergranular fracture observed in the HAZ region was caused by the growth of helium bubbles at grain boundaries. The bubbles grow, reducing the load bearing area of the grain boundaries until failure occurs. The growth kinetics of bubbles of insoluble gas are influenced by both temperature and stress. The bubble growth processes in the HAZ may be separated into three sequential regimes. Regime one is the heat-up period before the fusion occurs. Regime two occurs when molten metal is present in the fusion zone resulting in a stress-free state. Regime three occurs after the molten metal has begun to re-solidify and internal shrinkage stresses are

generated in the constrained plates. It should be recognized that the precipitation of mobile, interstitial helium is not a viable process for bubble formation or growth in either regime. This is because the helium born in the material during tritium exposure has clustered into small bubbles as a result of the 400°C off-gassing treatment (helium bubble formation has been shown to occur in austenitic stainless steels upon annealing at 350°C [12]). Helium trapped in even small clusters is very strongly bound (binding energies of 3.5-4.0 eV [13]) and is not free to migrate at any temperature appreciably below the melting point.

In the first regime, the bubble will grow as a result of the generation of thermal vacancies during the heat-up period. However, the presence of compressive stresses will tend to delay bubble growth on grain boundaries normal to compressive stresses. Nevertheless, this heat-up period will nucleate bubbles if the degassing treatment did not do so. In the second regime bubble coarsening may occur by the migration of helium bubbles [14-16]. Since the solubility of helium in metals is negligible, coarsening via Ostwald ripening [17,18] processes are not likely to be of importance. Bubble growth is also known to occur from grain boundary migration [19] or from recrystallization. However, the prior annealing treatments at 1050°C insure that little driving force is available for such processes. Bubble growth may occur through the precipitation of vacancies into bubbles. Such a process is particularly favored at temperatures close to the melting point, since the vacancy concentration is

quite high. The driving force for bubble growth is provided by the interior helium gas pressure, $2\gamma/r$ where γ is the surface energy and r is the bubble radius. Since the initial small bubbles are likely to be non-equilibrium and highly overpressurized, this is a viable growth mechanism.

Once the material in the weld pool starts to solidify (regime 3), the kinetics of helium bubble growth will be controlled by the shrinkage stresses developed during cooling. Models of stress driven bubble growth have been extensively reviewed by Reidel [20]. In general, cavity growth is attributed to stress-driven diffusion of vacancies along grain boundaries to the bubble-grain boundary junction. The vacancy flux along the grain boundary is coupled to the flux along the internal cavity (bubble) surface so that an equilibrium cavity profile is maintained.

Formulating a rigorous model of bubble growth during a welding procedure is beyond the scope of the current work. However, the critical stress necessary to achieve unstable bubble growth can be estimated. This critical stress is given by $\sigma = 0.76 \gamma/r$ [21]. For stresses greater than this, growth will continue indefinitely causing coalescence with resulting intergranular failure. Murr et. al [22] reported a surface energy for stainless steel of 2.74 J/m^2 at 700°C . 40 nm diameter bubbles have been observed in 316L stainless steel containing 33 appm helium subsequent to an 850°C anneal [23]. From these values, a critical stress is calculated to be approximately 50 MPa. This is considerably below the measured yield strength of

the welded, He-doped material at the highest temperatures examined. Thus it is not unreasonable to suggest that the tensile shrinkage stresses generated during cooling are sufficient to promote bubble growth and that these bubbles will continue to grow until they coalesce and intergranular failure occurs or until temperature falls below the growth range.

Weld Response, Fusion Zone

Weld crack features of the fusion zone of the 105 appm welded material (Figure 3d) reveal that brittle fracture occurred along interdendritic paths. Metallography of the fusion zone (Figure 5) suggests that brittle failure had its origins in the precipitation of helium bubbles in the dendritic boundaries. As solidification proceeds, helium is rejected by the growing dendrites because of the low solubility of helium in the metal and is trapped in the interdendritic region which is the last to solidify. These bubbles coalesce into microcracks. Tensile stresses developed in the weld during cooling then cause these cracks to propagate.

Mechanical Properties

Tensile test results indicate that the helium concentrations studied did not significantly degrade the mechanical properties of the materials for temperatures at and below 600°C (Figures 6 through 8). The increase in the yield strength of the welded materials relative to unwelded specimens, though not studied in detail, may be attributed to three possible mechanisms: an

increase in the dislocation density from deformation induced by shrinkage stresses, the development of second phase precipitates, and grain refinement in the fusion zone. It was found that annealing at 1050°C for one hour restored the yield strength to the value for parent material. The lower UTS observed in the welded He-doped material compared with the un-doped material is believed to have resulted from the onset of fracture prior to achieving any significant amount of work hardening by plastic deformation. Indeed, as shown in Figure 8 and Table 2, the welded specimens containing helium were unable to sustain any appreciable amount of plastic deformation. This loss of ductility of the welded, doped material is attributed to deformation induced growth and coalescence of helium bubbles along grain boundaries. Such a situation would be intolerable for a weld-repaired containment vessel or another load-bearing structure.

CONCLUSIONS

The following conclusions were drawn from the present study:

- o Severe intergranular cracking occurred during GTA welding of type 316 stainless steel plates containing helium concentrations of 27 and 105 appm.
- o Brittle fracture in both fusion and heat-affected zones was induced by the precipitation of helium bubbles at dendrite interfaces and by the growth and coalescence of He bubbles at grain boundaries.
- o The size and density of pores in the fusion zone increased

with increasing helium concentration. The largest pores and highest density of resolvable pores were found in the fusion zone near the fusion line.

- o After welding, He-doped materials exhibited poor tensile properties with ductilities close to zero. Fracture in these specimens was intergranular due to the plastic growth of grain boundary He bubbles.

The results indicate that repair or replacement of irradiated structural components containing relatively small amounts of helium using conventional GTA welding techniques will be difficult in stainless steel. Furthermore, even if such repairs can be made, the very low ductility welds may still impose a severe risk for components which must serve at elevated temperatures under conditions of creep or fatigue loading.

REFERENCES

1. R. S. Barnes, "Embrittlement of Stainless Steels and Nickel-Based Alloys at High Temperature Induced by Neutron Radiation," *Nature*, 206 (1965) pp.1307-1310.
2. D. R. Harries, "Neutron Irradiation-Induced Embrittlement in Type 316 and Other Austenitic Steels and Alloys," *J. Nucl. Mater.* 82 (1979) pp. 2-21.
3. J.v.d. Driesch and P. Jung, "An Investigation on the Solubility of Helium in Nickel," *High Temperature - High Pressure*, 12 (1980), pp. 635-641.
4. J. Laakmann, P. Jung and W. Uelhoff, "Solubility of Helium in Gold," *Acad Metall.*, 35 (1987), pp. 2063-2069.

5. S. L. Robinson, "Tensile Properties of Welded Helium Charged 304L Stainless Steel," in print, J. Nuc. Mater.
6. J. P. Maloney, et al., "Repair of a Nuclear Reactor Vessel," DP-1199, E. I. du Pont de Nemours & Co., Savannah River Laboratory, Aiken, SC, (June 1969).
7. "Safety Issues at the Defense Production Reactors," Committee to Assess Safety and Technical Issues at DOE Reactors, Commission on Physical Science, Mathematics and Resources and the Commission on Engineering and Technical Systems, National Research Council, National Academy Press, Wash. D. C., 1987.
8. B. A. Chin, R. J. Neuhold and J. L. Straalsund, "Materials Development for Fast Breeder Reactor Cores," Nucl. Technol., 57 (1982) pp. 426-435.
9. Annual Books and ASTM Standards. Vol. 12.02, E 942 - 83 pp. 808-811.
10. M. R. Louthan, Jr. and R. G. Derrick, "Hydrogen Transport in Austenitic Stainless Steel," Corrosion Science, 15 (1975) pp. 565-577.
11. B. M. Oliver, J. G. Bradley and H. Farrar IV, "Helium Concentration in the Earth's Lower Atmosphere," Geochim et Cosmochim. ACTA, 48 (1984), pp. 1759-1767.
12. S. L. Robinson, "Tritium and Helium Effects on Plastic Deformation in AISI 316 Stainless Steel," Mater. Sci. and Engr., 96 (1987), pp. 7-16.
13. M. I. Baskes and V. Vitek, "Trapping of Hydrogen and Helium at Grain Boundaries in Nickel: An Atomistic Study," Met.

- Trans., 16A (1985), pp. 1625-1631.
14. R. S. Barnes, "A Theory of Swelling and Gas Release for Reactor Materials," J. Nucl Mater., 11 (1964), pp. 135-148.
 15. E. E. Gruber, "Calculated Size Distribution for Gas Bubble Migration and Coalescence in Solids," J. Appl. Phys., 38 (1967), pp. 243-250.
 16. E. M. Baroody, "Calculation on the Collisional Coalescence of Gas Bubbles in Solids," J. Appl. Phys., 38 (1967), p.4893-4903.
 17. G. W. Greenwood and A. Boltax, "The Role of Fission Gas Resorption During Post-Irradiation Heat Treatment," J. Nucl. Mater., 5 (1962), pp 234-240.
 18. A. J. Markworth, "On the Coarsening of Gas-Filled Pores in Solids," Met. Trans., 4A (1973), pp. 2651-2656.
 19. W. Beere, "The Growth of Sub-Critical Bubbles on Grain Boundaries," J. Nucl. Mater., 120 (1984), pp. 88-93.
 20. H. Reidel, Fracture at High Temperature, Springer-Verlag, New York, 1987.
 21. E. D. Hyam and G. Sumner, "Irradiation Damage to Beryllium," Proc. Conf. Radiation Damage in Solids, Vol. 1 (IAEA, Vienna, 1962) pp. 323-331.
 22. L. E. Murr, G. I. Wong and R. J. Horylev, "Measurement of Interfacial Free Energies and Associated Temperature Coefficients in 304L Stainless Steel," Acta Metall., 21 (1973), pp. 595-604.
 23. S. H. Goods, unpublished work.

Table 1. Chemical Composition for Reference Heat (8092297) of Type 316 Stainless Steel.

Element	Content, wt %
C	0.057
Mn	1.86
P	0.024
S	0.019
Si	0.58
Ni	13.48
Cr	17.25
Mo	2.34
Co	0.02
Cu	0.10
N	0.03
B	0.0005
Ti	0.02
Pb	0.034
Sn	0.004

Table 2. Tensile Test Data of Type 316 Stainless Steel.

Material	Temp (°C)	UTS (MPa)	Y.S. (MPa)	% Elong
Control (unwelded)	20	584.5	231.5	44.1
	20	580.1	223.5	45.2
	500	466.4	123.2	26.0
	500	487.5	124.8	25.2
	600	458.3	103.7	26.8
	600	447.0	104.6	27.2
	700	357.0	98.5	23.7
	700	340.3	99.1	21.0
27 appm	20	549.7	190.1	37.8
	500	481.2	141.0	25.0
	600	458.3	117.4	25.1
	700	372.7	123.0	15.9
105 appm	20	583.0	244.5	39.8
	500	494.0	149.0	27.1
	600	456.1	121.0	26.1
	700	328.4	126.4	11.3
Control ¹ (welded)	20	560.2	351.2	17.8
	20	569.1	347.8	18.5
	500	387.5	244.2	7.2
	500	408.9	232.5	10.3
	600	369.7	222.3	6.0
	600	357.3	211.0	8.1
	700	325.0	197.5	7.7
	700	291.0	175.0	9.1
27 appm ²	20	386.0	386.0	0.2
	500	296.4	266.8	0.6
	600	262.8	227.6	1.2
	700	200.0	191.0	0.3
105 appm ²	20	404.0	373.0	1.5
	500	261.9	253.9	1.4
	600	253.1	244.1	0.6
	700	199.6	191.5	1.2

1. Specimens failed in the fusion zone.
2. Specimens failed at the fusion boundary.

CAPTIONS:

- Figure 1. Experimental welding station.
- Figure 2. Morphological Features of As-Welded Material: Helium Level 27 appm. (a). Macrograph of Heat-Affected Zone Showing Intergranular Fracture. (b). Scanning Electron Micrograph Showing Details of Intergranular Fracture. (c). Scanning Electron Micrograph of Grain Boundary Facets Decorated with a Uniform Distribution of Dimples.
- Figure 3. Morphological Features of As-Welded Material: Helium Level 105 appm. (a). Macrograph of Brittle Fracture in Heat-Affected and Fusion Zones. (b). Scanning Electron Micrograph Showing Details of Intergranular Fracture. (c). Scanning Electron Micrograph of Grain Boundary Facets Decorated with a Uniform Distribution of Dimples. (d). Scanning Electron Micrograph Showing that Brittle Failure Proceeded along an Interdendritic Path.
- Figure 4. Optical Micrographs of Welds Taken Transverse to the Welding Direction. (a). Control Material. (b). 27 appm. (c). 105 appm. Failure Occurred in the Heat-Affected Zone. Larger Pore Size and Greater Density of Helium Bubbles Occurred in the Fusion Zone near the Fusion Line.
- Figure 5. SEM Micrographs of the Fusion Zone. (a). Control Material. (b). 27 appm. (c). 105 appm.
- Figure 6. Temperature and Helium Concentration Dependence of Yield Strength.
- Figure 7. Temperature and Helium Concentration Dependence of Ultimate Tensile Strength.
- Figure 8. Temperature and Helium Concentration Dependence of Total Elongation.
- Figure 9. Scanning Electron Micrographs of welded 27 appm material Tested at 25°C. (a). Intergranular Fracture. (b). Feature Showing Uniform Distribution of Dimples.

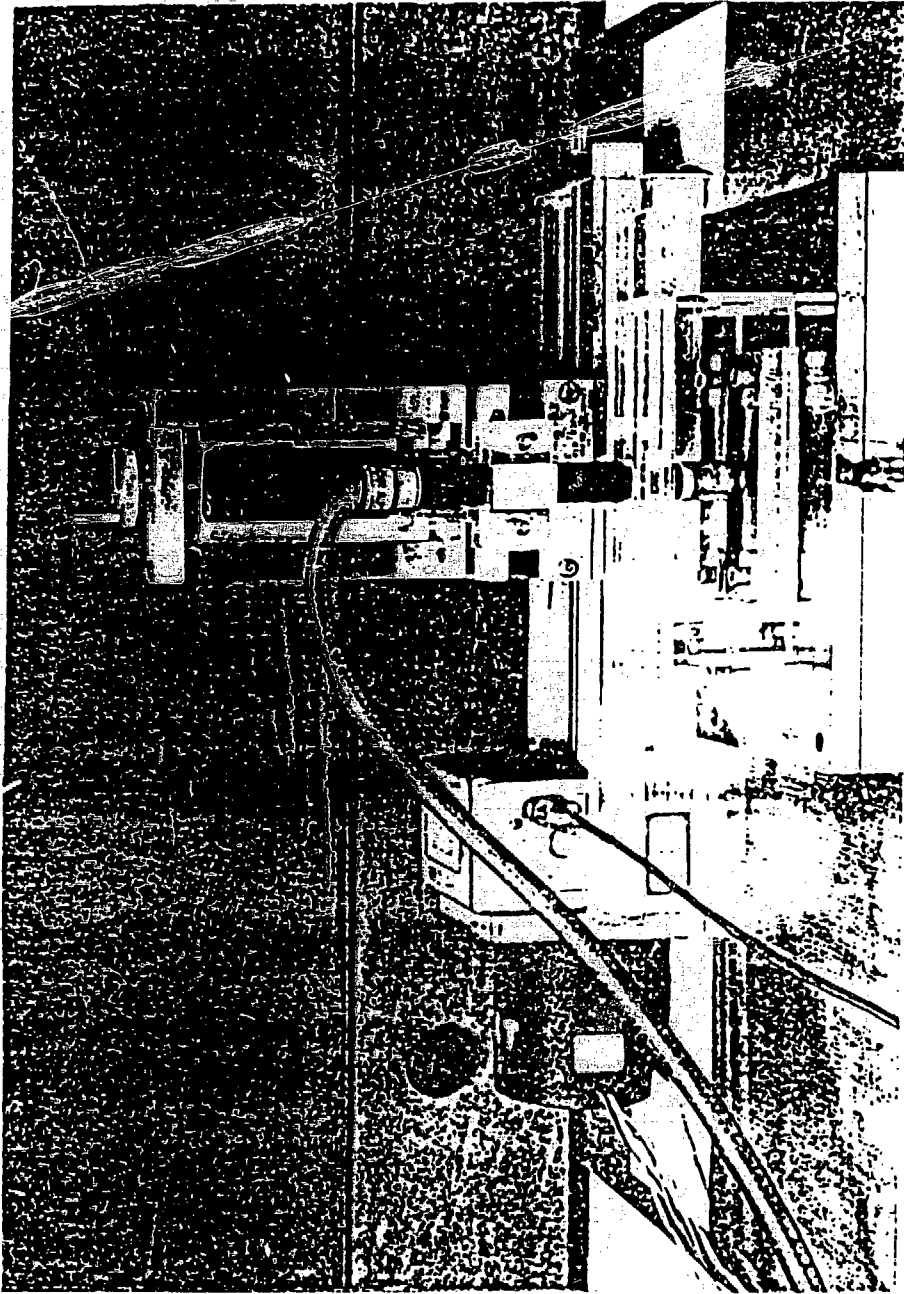


Figure 1

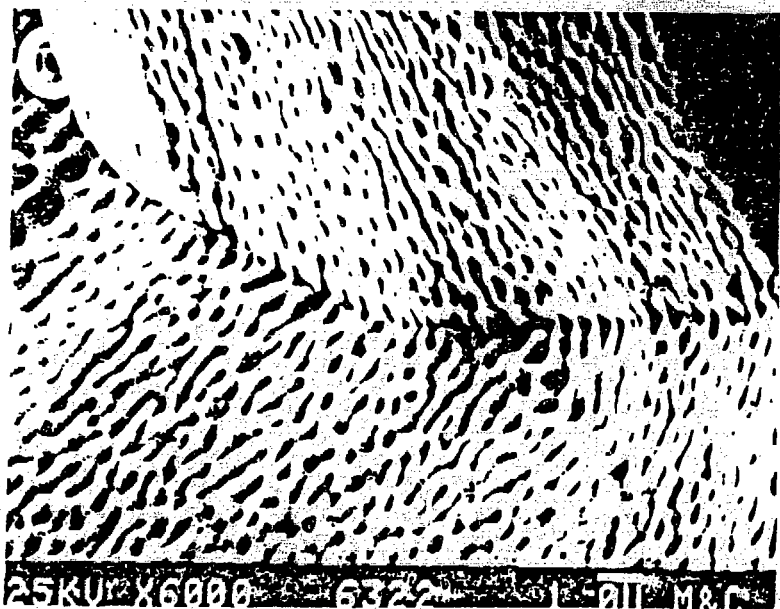
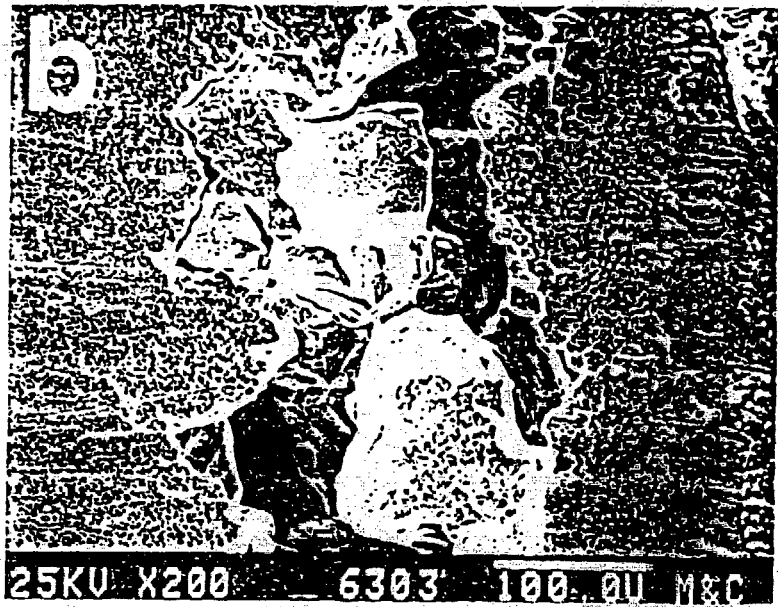
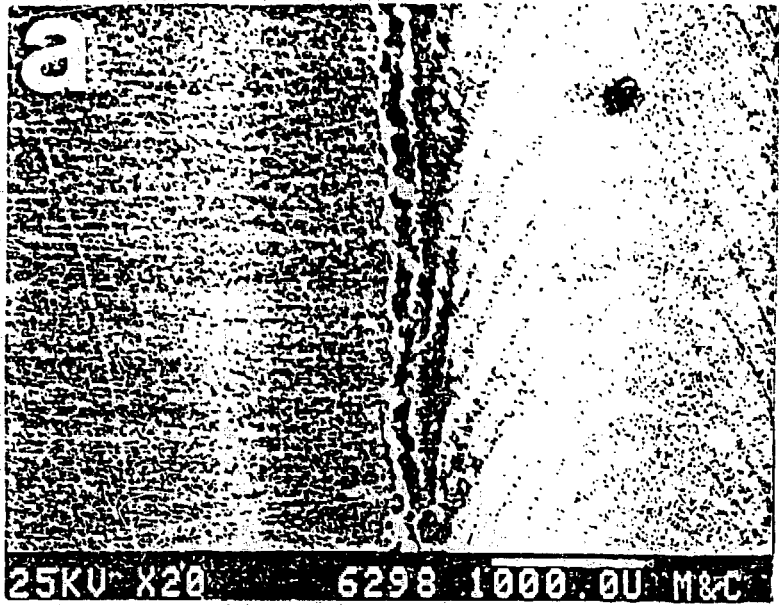


Figure 2

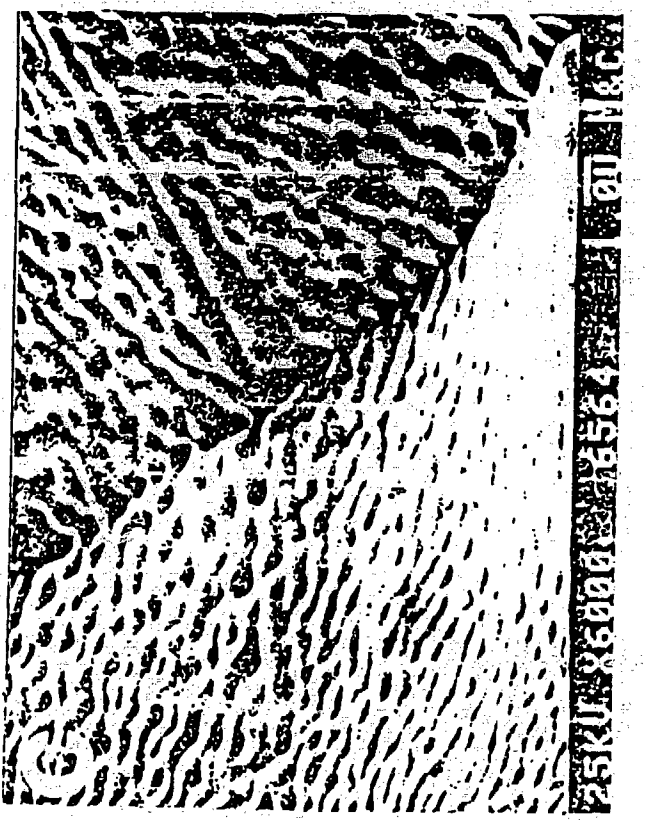
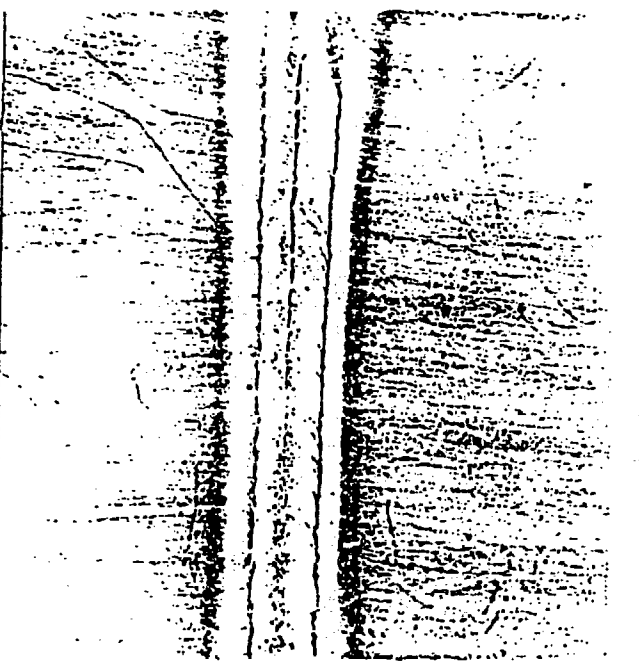
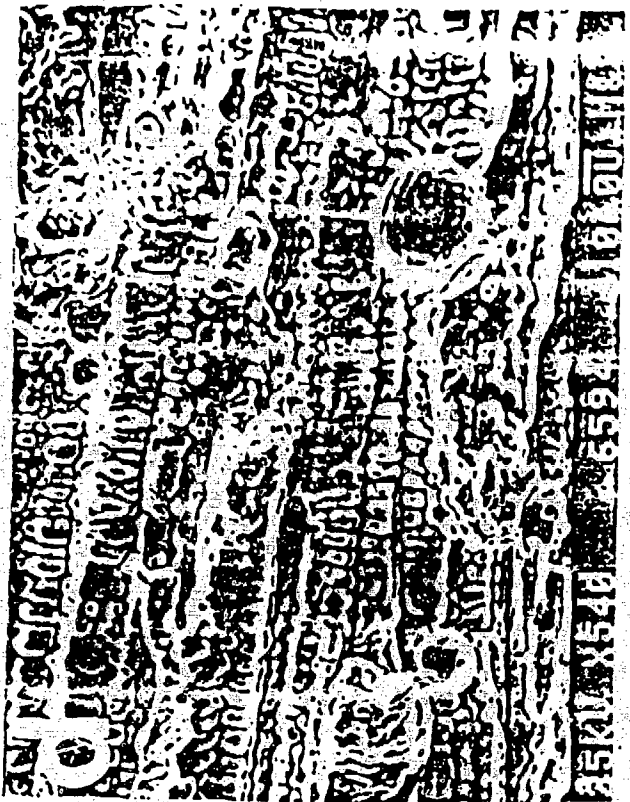
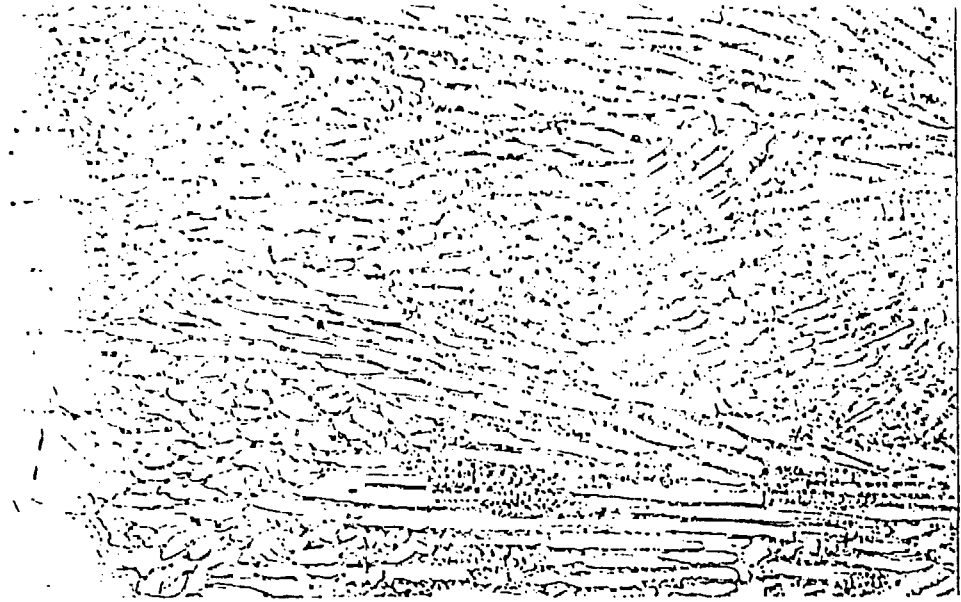


Figure 3

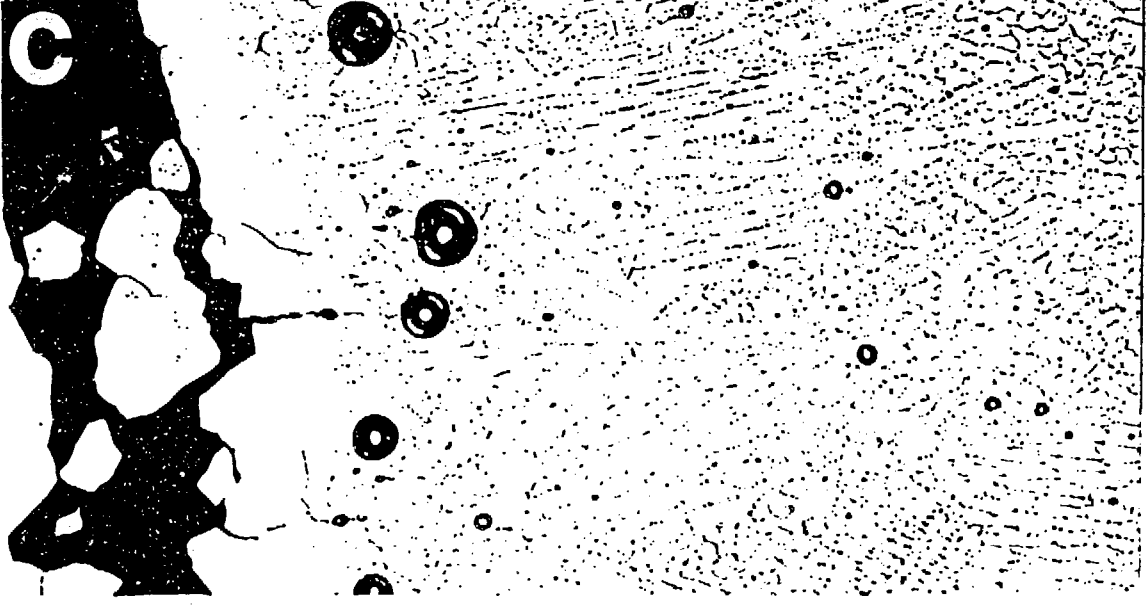
a



b



c



100 μ m

200X

Figure 4

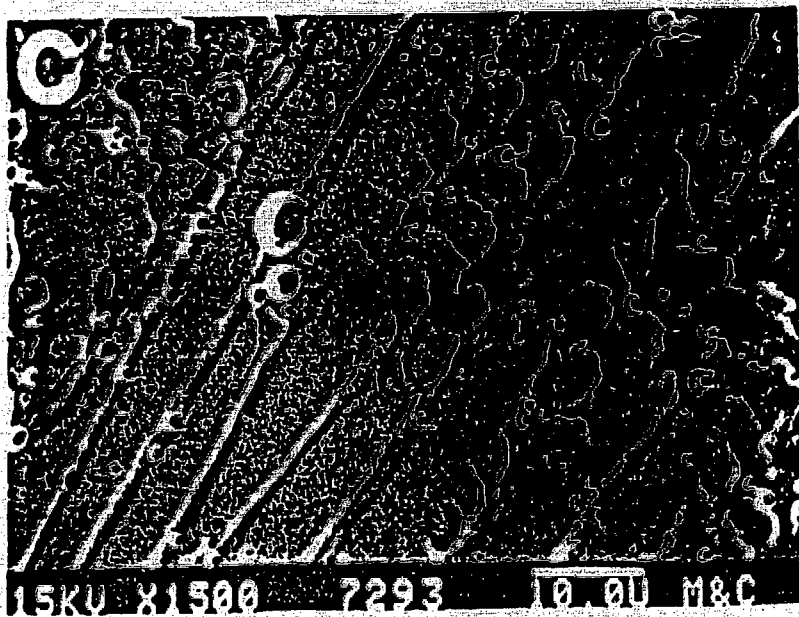
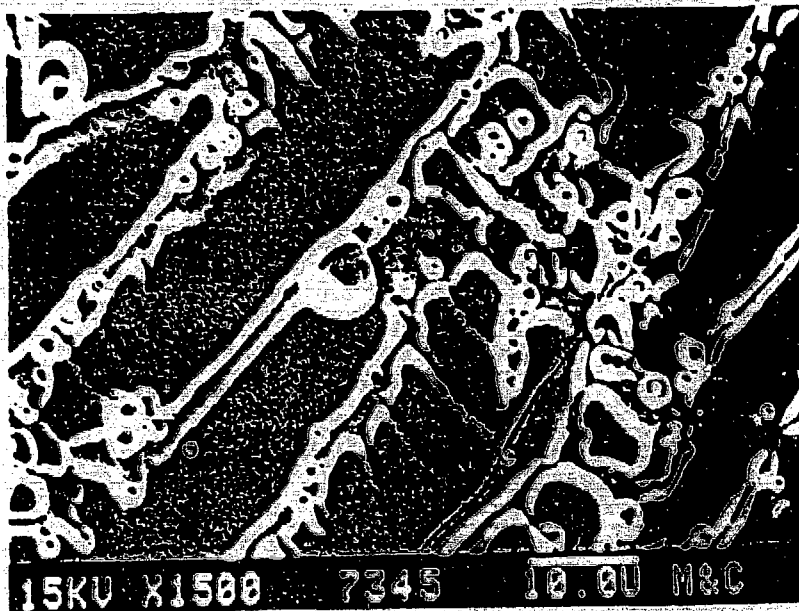
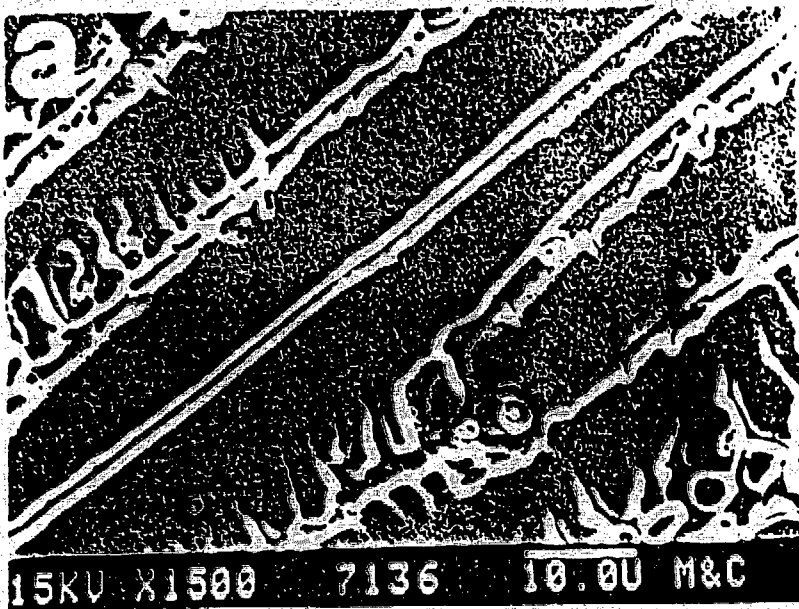


Figure 5

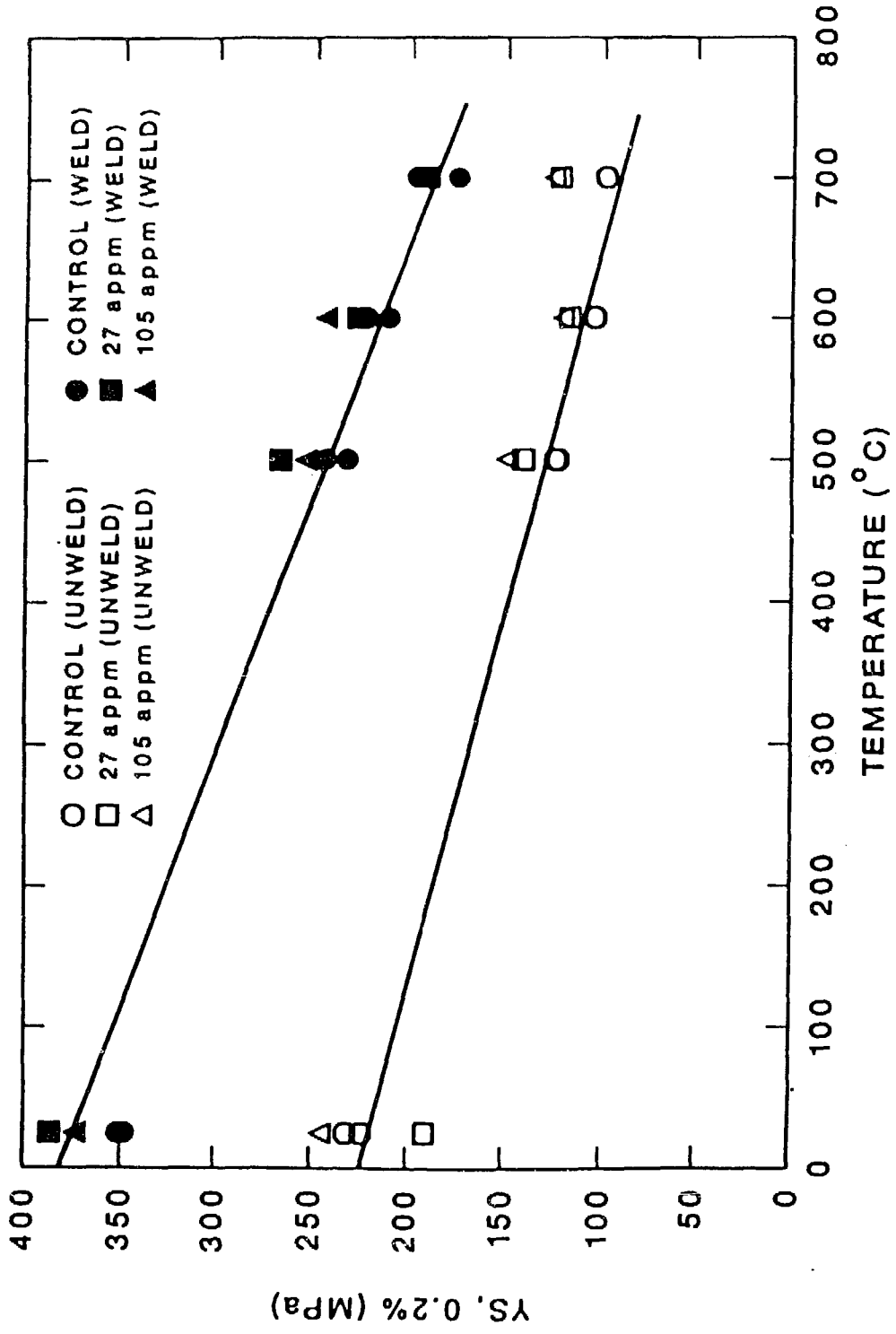


Figure 6

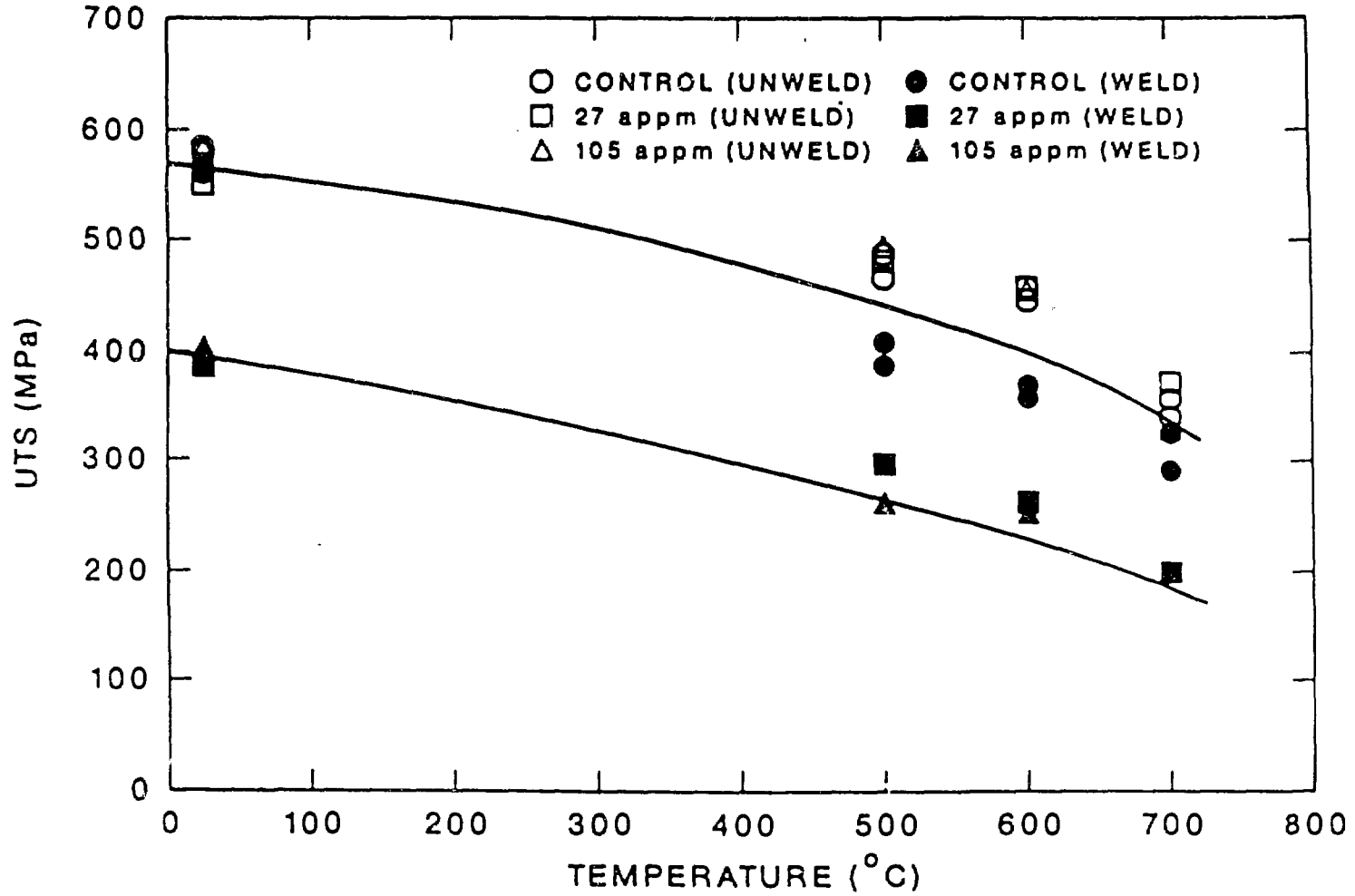


Figure 7

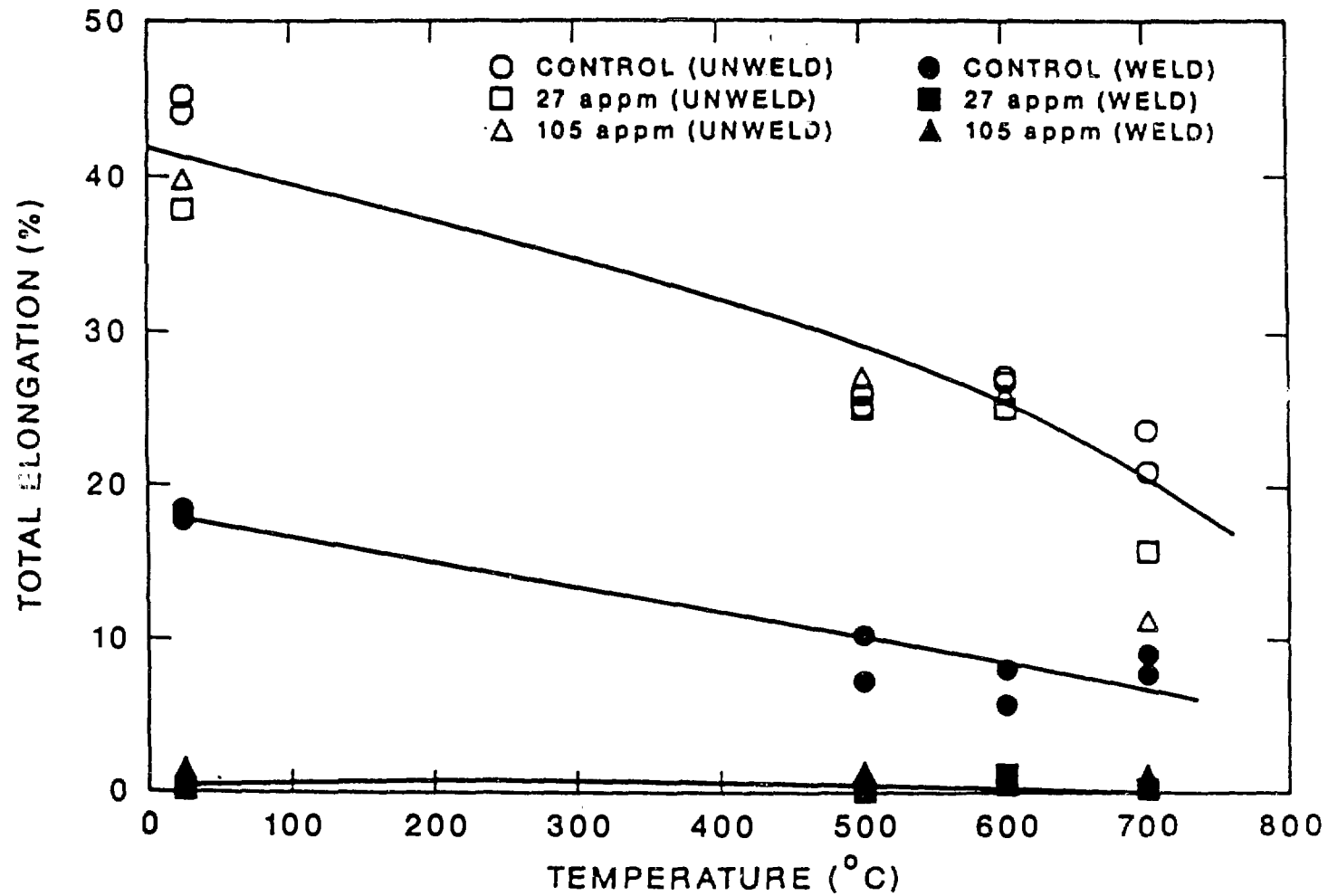


Figure 8

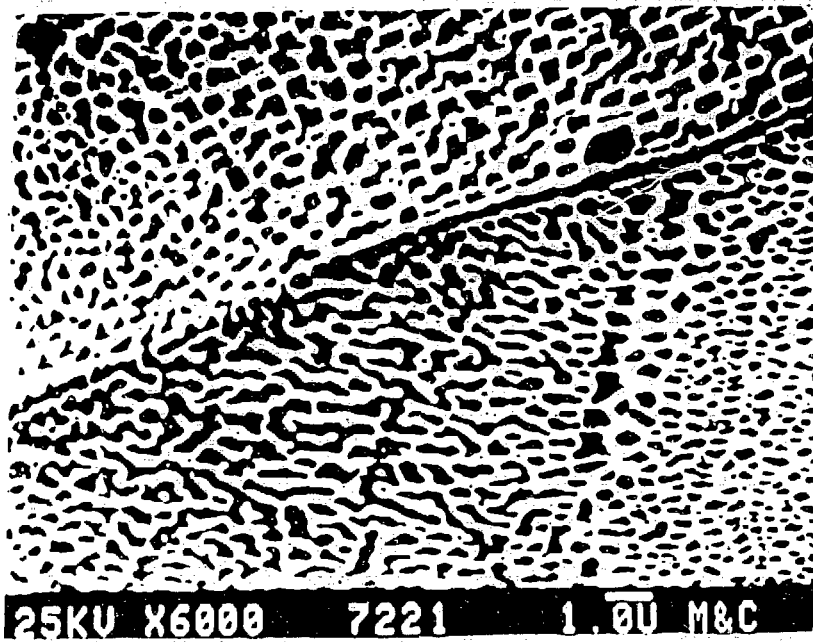
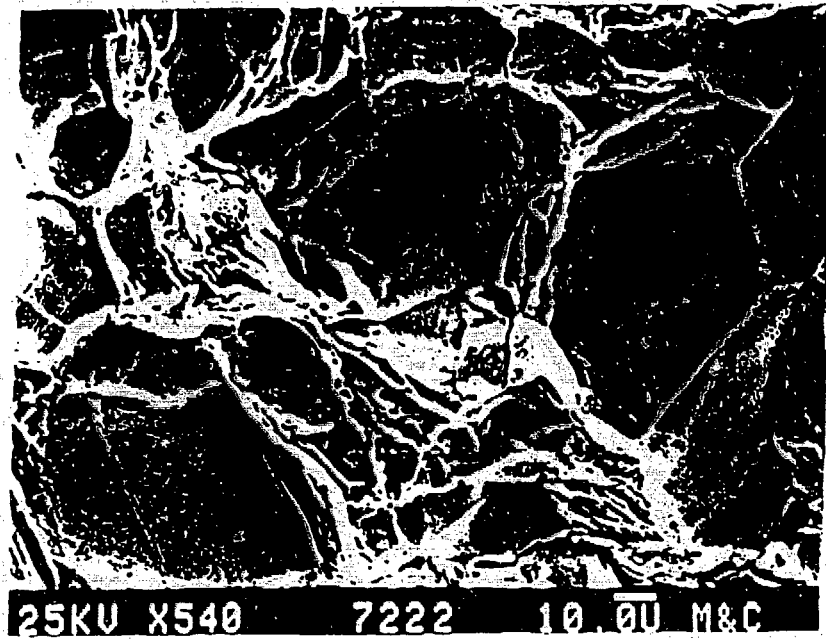


Figure 9